Solid State Communications 250 (2017) 53–56

Contents lists available at ScienceDirect

Solid State Communications

journal homepage: www.elsevier.com/locate/ssc

Communication

Dielectric relaxation in AC powder electroluminescent devices

Shuai Zhang[a,*], Haibin Su[b], Chuan Seng Tan[a], Terence Kin Shun Wong[a], Ronnie Jin Wah Teo[c]

[a] School of Electrical and Electronic Engineering, Nanyang Technological University, 639798, Singapore
[b] School of Materials Science and Engineering, Nanyang Technological University, 639798, Singapore
[c] Singapore Institute of Manufacturing Technology, ASTAR, 638075, Singapore

A B S T R A C T

The dielectric properties of AC powder electroluminescent devices were measured and analyzed using complex impedance spectroscopy to determine the relaxation processes occurring within the devices. The relaxation processes identified were ascribed to the electrode polarization caused by ion accumulation at the electrode/resin interfaces, the Maxwell-Wagner-Sillars effects at the (ZnS or $BaTiO_3$) particle/resin interfaces, and the dipolar reorientation of polymer chains in the resin matrix. Each relaxation process was represented by its corresponding equivalent circuit component. Space charge polarization at the electrodes were represented by a Warburg element, a resistor, and a constant phase element. The resin matrix, ZnS/resin and $BaTiO_3$/resin interfaces could each be modeled by a resistor and a capacitor in parallel. The simulated equivalent circuits for three different printed structures showed good fitting with their experimental impedance results.

1. Introduction

AC powder electroluminescent devices (ACPELDs) were first made by Destriau [1] and are now widely adopted in back lighting applications such as automotive dashboards and LCD displays. Recently, these devices have been applied to new fields such as paper display [2], interactive packaging [3], and stretchable displays [4]. Conventional ACPELDs are printed with light emitting and dielectric layers sandwiched in between transparent and back electrodes. The light emitting layer typically consists of ZnS microparticles mixed with resin while the dielectric layer and back electrode contain $BaTiO_3$ and Ag/C nanoparticles in resin respectively. ACPELDs are generally assumed to be capacitive by nature, borne out from a resistor (R) and capacitor (C) circuitry. Various simplified RC-based equivalent circuit models have been proposed in order to understand the operational characteristics of ACPELDs. Bredol and Dieckhoff demonstrated that ACPELDs could be represented by a capacitive load with series and shunt resistors [5]. The shunt and series resistors represent the direct current (DC) conductivity of ACPELDs and resistivity of the contacts, respectively. Winscom et al. proposed an equivalent circuit model with effective R and C components in a series configuration [6]. They suggested that the effective capacitance was governed by the dielectric material and the phosphor particles were accountable for the effective resistance in the single-layer ACPELDs. However, the equivalent circuit for ACPELDs is more complex with the consideration of the microscopic features and interfaces [7].

ACPELDs are a complex composite system with several layers of polymer composites stacking above each other. A dielectric layer is typically printed over a light emitting layer, which typically contains ZnS microparticles, to increase the electrical field surrounding the ZnS microparticles during electrical excitation and, in turn, increase its light emission properties. The incorporation of micro- or nanoparticles into a polymeric material will introduce interfacial polarization or Maxwell-Wagner-Sillars (MWS) effect at the particle/matrix interfaces and enhance the dielectric performance of the polymer composite material [8,9]. In this paper, complex impedance spectroscopy was employed to obtain the dielectric properties of ACPELDs. In order to segregate the types of relaxation processes in the device, the dielectric properties of the composite films containing either a dielectric layer or a light emitting layer were also measured and compared with those of ACPELDs. From the impedance data, equivalent circuit models were subsequently proposed for different printed device structures.

2. Experimental details

The three different device architectures fabricated using screen printing process were: dielectric film (indium tin oxide (ITO)-coated polyethylene terephthalate (PET)/$BaTiO_3$/Ag), phosphor film (ITO-coated PET/ZnS/Ag) and ACPELDs (ITO-coated PET/ZnS/$BaTiO_3$/Ag). Depending on the device architecture, either ZnS microparticles (mean particle size ~20 μm) or $BaTiO_3$ nanoparticles (mean particle size ~100 nm) pre-mixed with polymeric resin were printed onto an

* Corresponding author.
E-mail address: sazhang@ntu.edu.sg (S. Zhang).

http://dx.doi.org/10.1016/j.ssc.2016.11.010
Received 11 April 2016; Received in revised form 6 October 2016; Accepted 12 November 2016
Available online 14 November 2016
0038-1098/

ITO-coated PET film. Ag nanoparticle pastes were subsequently printed to form the back electrode. The impedance spectra were measured in potentiostat mode over a frequency range of 10^{-2}–10^5 Hz at 90 °C using Autolab PGSTAT302N. The temperature control was achieved through a thermoelectric heater. The equivalent circuits were simulated and fitted using both Nova (Autolab) and Zview software.

To obtain the permittivity and electric modulus, the absolute capacitances (the capacitance of the empty cell) for the dielectric film, phosphor film, and ACPELDs are calculated using the following equation:

$$C_c=\frac{\varepsilon_0 A_c}{l} \tag{1}$$

where ε_O is the vacuum permittivity and A_c is the device area, which is 0.01 m^2. The thicknesses (l) of the dielectric film, phosphor film and ACPELDs are 31 μm, 52.4 μm and 56.5 μm respectively as measured through SEM imaging. The real (ε') and imaginary (ε'') parts of the dielectric permittivity can be calculated through the measured real (Z') and imaginary (Z'') parts of the complex impedance [10]:

$$\varepsilon'=\frac{-Z''}{2\pi f C_c(Z''^2+Z'^2)} \tag{2}$$

$$\varepsilon'' = \frac{Z'}{2\pi f C_c(Z''^2+Z'^2)} \tag{3}$$

where f is the frequency of the applied AC voltage.

3. Results and discussion

Fig. 1(a) shows the imaginary permittivity ε'' as a function of frequency for the dielectric film, phosphor film and ACPELDs. ε'', which represents the dielectric loss factor of the material and follows the relationship $\varepsilon'' = \sigma/2\pi\varepsilon_0 f$ [11], exhibits an inverse proportional relationship with frequency at the low frequency range. The bulk electrical conductivity σ is caused by the migration of ionic carriers [12]. At low frequencies, ions can travel over long distances and form a DC conduction path, which contributes to the linearity in the ε''-f curve. Its mobility decreases with frequency until its ionic movement becomes locally confined.

Similar to the ε''-f curves, the real permittivity ε' in Fig. 1(b) also shows an inverse proportional relationship with frequency till its critical frequency f_c'. The f_c' values for the dielectric film, phosphor film and ACPELDs are 0.037 Hz, 1 Hz and 0.14 Hz respectively. As mentioned earlier, mobile ions are the main contributor to the direct current at low frequencies. If the mobile ions exchange all the charges at the electrodes, electrical neutrality should be maintained in the device and ε' should stay constant at low frequencies. However, the continuous increase of ε' with the decrease of frequency indicates that charges are exchanged partially and, hence, hetero space charge layers are formed at the vicinity of the electrodes. This phenomenon is called electrode polarization (EP) and were found to be present in all the three devices. Based on the f_c' values, the phosphor film exhibits the shortest relaxation time with the dielectric film have the longest relaxation duration.

To identify other possible relaxation processes present in the

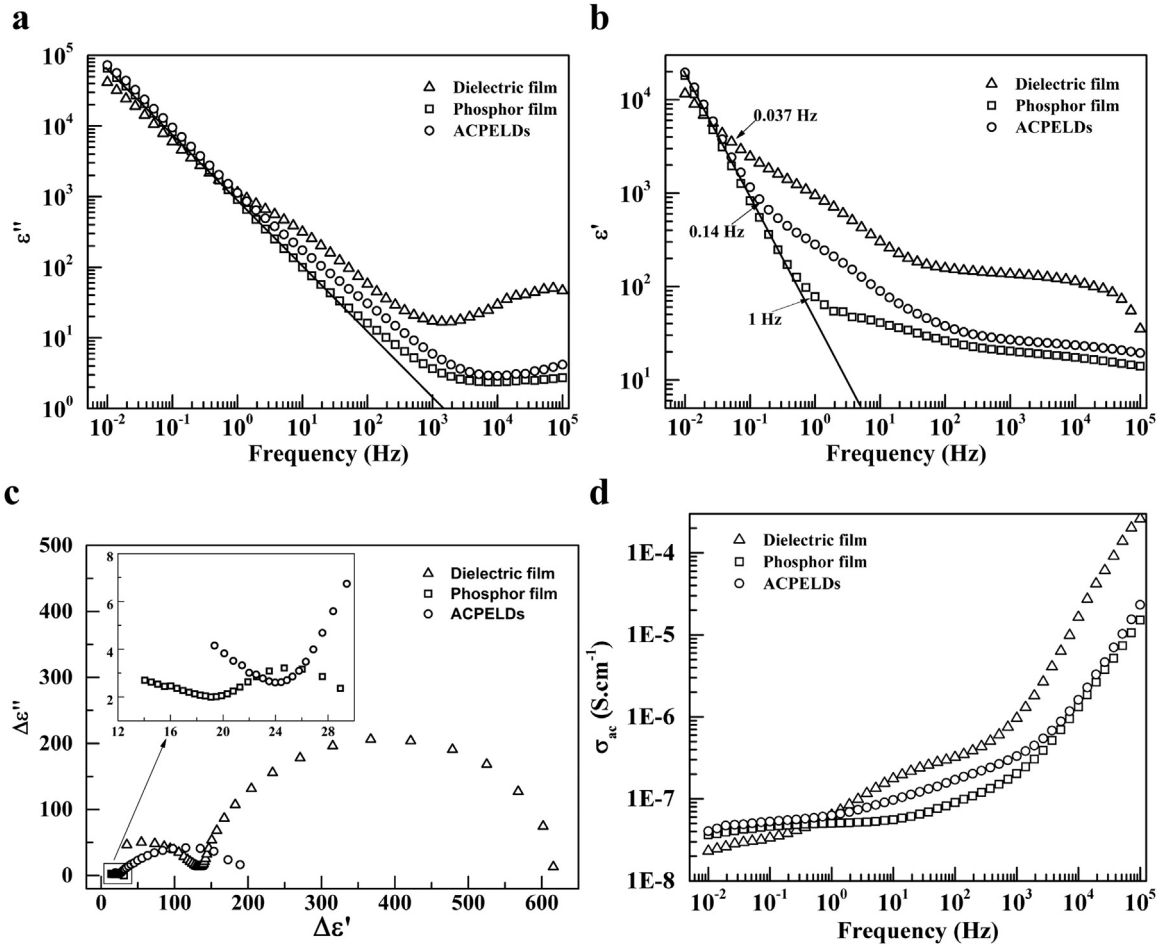

Fig. 1. (a) Imaginary (ε'') and (b) real (ε')part of permittivity and (d) real part of ac conductivity as function of frequency observed for the dielectric film, phosphor film and ACPELDs. (c) Imaginary part ($\Delta\varepsilon''$) of relative permittivity as a function of real part ($\Delta\varepsilon'$) of relative permittivity for the dielectric film, phosphor film and ACPELDs.

phosphor and dielectric layers, the relative permittivity is plotted for the dielectric film, phosphor film and ACPELDs as shown in Fig. 1(c). By subtracting the components of ε' and ε'' contributed by ionic conduction, the direct current and EP are significantly reduced. All three devices exhibit a small arc at low $\Delta\varepsilon'$ followed by a big semi-circle at high $\Delta\varepsilon'$. The small arc is attributed to the dipolar reorientation of polymer chains in the resin matrix and the big semi-circle is due to the MWS effect at the particle/resin interfaces [13]. As such, the MWS effect in the dielectric film is at the $BaTiO_3$/resin interface while that in the phosphor film occurs at the ZnS/resin interface. However, the MWS effect in the dielectric film is much more significant than that in the phosphor film. This is due to the larger surface-to-volume ratio of $BaTiO_3$ nanoparticles in the resin matrix as compared to the ZnS microparticles. It is also observed that the MWS effect and dipolar polarization in the ACPELDs falls in between the dielectric film and phosphor film and is considered as the superposition of the two films. In the low and high frequency regions, the AC conductivities of the phosphor film and ACPELDs are close as shown in Fig. 1(d). In the intermediate frequency region, the AC conductivity of ACPELDs is considered as the superposition of the two films. At frequencies above 1 Hz, it is expected that the dielectric film exhibits a higher σ_{ac} due to the more significant interfacial charges experienced at the $BaTiO_3$/rein interfaces.

The loss tangent tan δ, which quantifies the material's inherent dissipation of electromagnetic energy, for the dielectric film, phosphor film and ACPELDs is shown in Fig. 2(a). The tan δ spectra shows the polarization effects taking place according to its relaxation frequency. As shown in Fig. 2(a), the more significant MWS effect at the $BaTiO_3$/resin interface causes the higher tan δ in the dielectric film and ACPELDs than in the phosphor film. At high frequencies, polarization due to dipolar reorientation of resin at high frequencies is also found. Polarization in the resin matrix caused by the dipolar reorientation of polymer chains in the phosphor film is more significant than in the dielectric film. This may be attributed by the higher volume fraction of resin in the ZnS layer as compared to the $BaTiO_3$ layer. The presence of this polarization in the resin matrix was further analyzed using the complex electric modulus as shown in Fig. 2(b). It represents the true relaxation processes in the bulk material with the EP being suppressed [11]. At intermediate frequencies, M'' peaks are observed for all the three devices and Kontos et al. [14] attribute this M'' response to the macromolecule orientation of polymeric resin (α-mode). At high frequencies, there is a tendency to form another relaxation peak. Patsidis and Psarras showed similar characteristics and suggested that the high frequency relaxation process is attributed to the relaxation of segmental chains or side chains of resin (β-mode) in their $BaTiO_3$ polymer composite material [15]. Consequently, the dipolar polarization in the resin matrix is contributed by both α-mode and β-mode relaxations.

From the above analyses, three relaxation processes caused by different polarization mechanisms are found: EP due to ion accumulation at the electrodes, dipolar reorientation of polymer chains in the resin matrix, and MWS effects at the particle/resin interfaces. The MWS effect occurs at their respective ZnS/resin and $BaTiO_3$/resin interfaces. To better illustrate these relaxation processes, an equivalent circuit is constructed for each device. Using this equivalent circuit, the simulated Nyquist plots are compared with its experimental impedance data. As shown in Fig. 3, close fittings with a standard deviation of less than 5% are obtained for all three devices.

In Fig. 3(a), the equivalent circuit for the dielectric film models the relaxation processes contributed by the resin matrix, $BaTiO_3$ nanoparticles and electrodes. R_s is the series resistance of the electrodes. Polarization due to the dipolar reorientation of resin matrix can be represented by a resistor (R_m) and capacitor (C_m) in parallel, which describes the conductivity and the dipolar polarization of the resin polymer chains. Another parallel resistor (R_{bto}) and capacitor (C_{bto}) component is used to model the MWS effect at the $BaTiO_3$/resin interfaces and also depicts the conductivity and charge accumulation level at the interfaces. The last portion of the equivalent circuit for the dielectric film describes the charge accumulation behavior at the electrode/resin interface. R_e is the resistance of the interface and represents the efficiency of charge transfer from ions to electrons and from resin matrix to the electrodes. A larger R_e can be understood as the ions having a lower efficiency in charge transfer, resulting in higher amount of ions accumulation at the interfaces. Z_w, the Warburg element, represents the diffusional properties of the mobile ions in the resin matrix towards the electrodes and is quantified by the Warburg admittance Y_{0w}. A smaller Y_{0w} value corresponds to lower diffusivity of the mobile ions in resin. CPE_e is the constant phase element (CPE) at the electrode/resin interface, which represents the imperfect capacitive nature of the interface. This imperfect capacitive phenomenon represents the distribution of time constants at the electrode/resin interface, which is mainly caused by the non-uniformity of the interface. In Fig. 3(b), the equivalent circuit for the phosphor film is identical to the dielectric film with the exception that the parallel RC (R_{ZnS} and C_{ZnS}) component stands for the MWS effect at the ZnS/resin interface instead. The equivalent circuit for ACPELDs can be treated as the superposition of the equivalent circuit of the dielectric and phosphor films as shown in Fig. 3(c).

4. Conclusions

In conclusion, the relaxation processes of ACPELDs were analyzed by complex impedance spectroscopy. Three types of polarization mechanisms were identified in ACPELDs: electrode polarization due to ion accumulation at the electrode/resin interfaces, MWS effect at the ZnS and $BaTiO_3$ particle/resin interfaces and polarization due to the

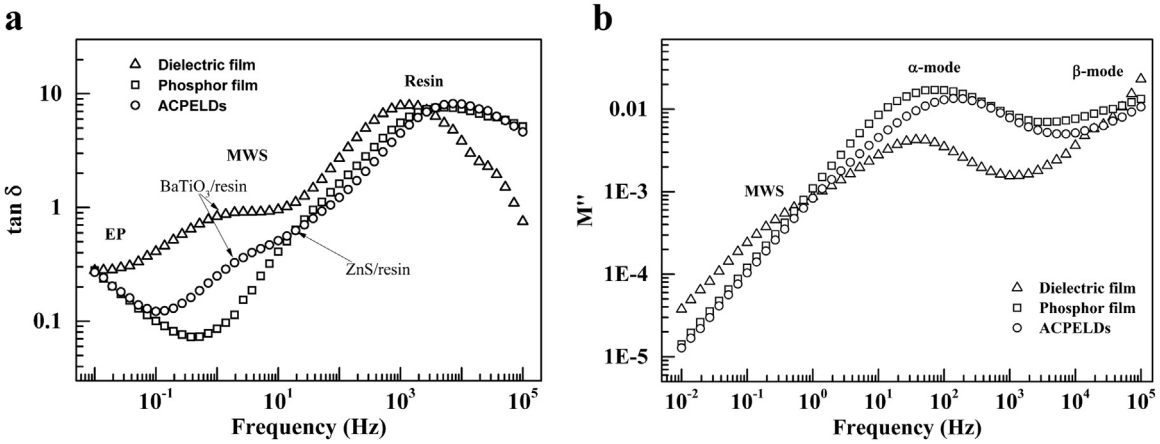

Fig. 2. (a) Loss tangent (*tan δ*) and (b) imaginary part (*M''*) of electric modulus as a function of frequency for the dielectric film, phosphor film and ACPELDs.

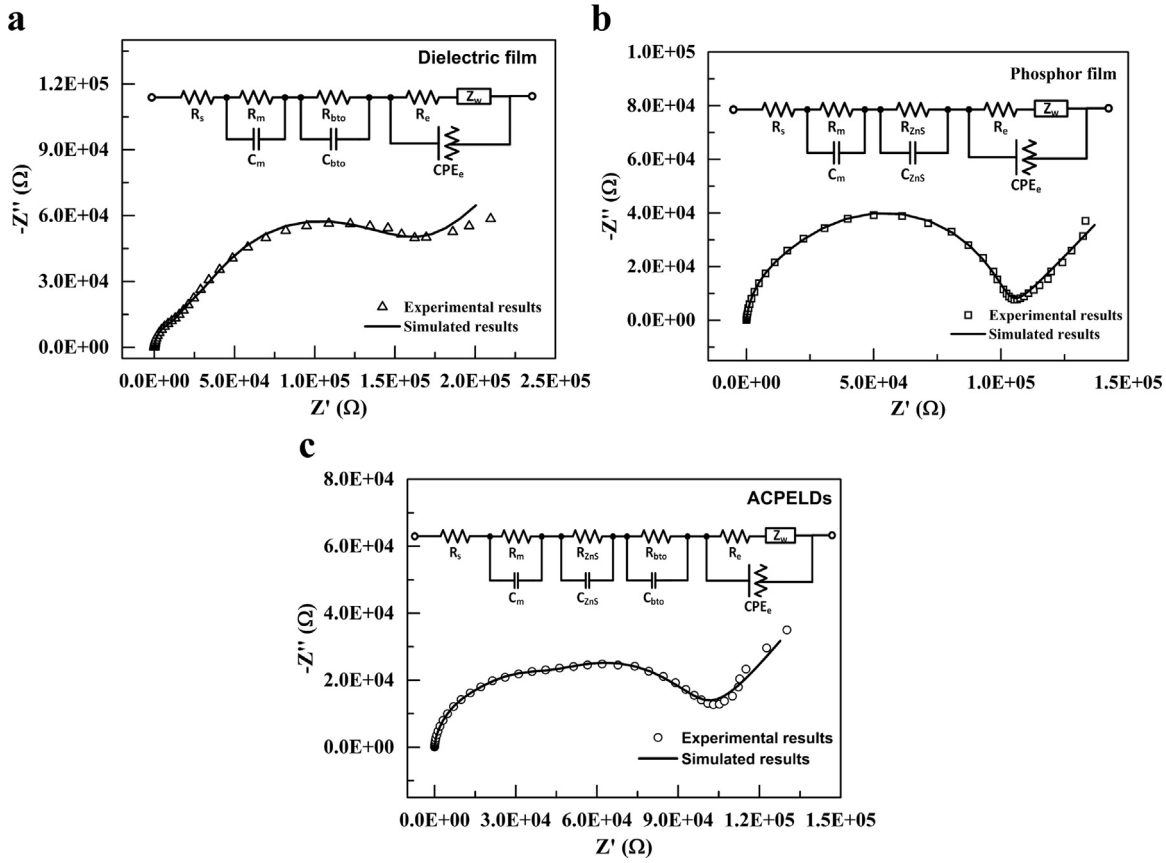

Fig. 3. Experimental and simulated Nyquist plots for the (a) dielectric film, (b) phosphor film and (c) ACPELDs with the corresponding equivalent circuit models. R_s: series resistance of the electrodes; R_m and C_m: resistance and capacitance of resin matrix; R_{ZnS} and C_{ZnS}: resistance and capacitance of the ZnS/resin interface; R_{bto} and C_{bto}: resistance and capacitance of the $BaTiO_3$/resin interface; *Re* and CPE_e: resistance and constant phase element of the electrode/resin interface; Z_w: Warburg element of the resin near the electrodes.

dipolar reorientation of polymer chains in the resin matrix. The MWS effect at the $BaTiO_3$/resin interface is much more significant than the ZnS/resin interface due to the smaller $BaTiO_3$ particle size. On the other hand, dipolar polarization of resin in the phosphor film is more significant than the dielectric film due to the larger volume fraction of resin in the phosphor layer. The dipolar polarization of resin consisted of both α-mode and β-mode. Finally, these polarization mechanisms were modeled using electrical circuit components and an equivalent circuit model for ACPELDs was derived. The simulated circuit model, which shows good fitting with its experimental results, provides a better understanding of the ACPELD architecture and enabled an effective non-destructive diagnosis of ACPELDs and other printed electronics applications.

Acknowledgments

The authors want to thank Singapore Institute of Manufacturing Technology (SIMTech) for the providing the device specimens as well as funding support for this project under grant number U14-P-040SU.

References

[1] G. Destriau, Recherches sur les scintillations des sulfures de zinc aux rayons, R. Bussière (1936).
[2] J.-Y. Kim, S.H. Park, T. Jeong, M.J. Bae, S. Sunjin, J. Lee, et al., Paper as a Substrate for inorganic powder electroluminescence devices, IEEE Trans. Electron Devices vol. 57 (2010) 1470–1474.
[3] G. Wroblewski, M. Sloma, D. Janczak, A. Mlozniak, and M. Jakubowska, "Electroluminescent structures with nanomaterials for direct printing of interactive packages and labels," in Electronics Technology (ISSE), in: Proceedings of the 2014 37th International Spring Seminar on, 2014, pp. 357–360.
[4] J. Wang, C. Yan, K.J. Chee, P.S. Lee, Highly stretchable and self-deformable alternating current electroluminescent devices, Adv. Mater. 27 (2015) 2876–2882.
[5] M. Bredol, H. Schulze Dieckhoff, Materials for powder-based AC-electroluminescence, Materials 3 (2010) 1353.
[6] C.J. Winscom, P.G. Harris, J. Silver, Equivalent circuits and efficacy of single-layer ACPEL Devices, ECS J. Solid State Sci. Technol. 3 (2014) R104–R108.
[7] H. Althues, J. Henle, S. Kaskel, Functional inorganic nanofillers for transparent polymers, Chem. Soc. Rev. 36 (2007) 1454–1465.
[8] G.C. Psarras, Conductivity and dielectric characterization of polymer nanocomposites, in: Y.W. Mid (Ed.)Physical Properties and Applications of Polymer Nanocomposites, Woodhead Publishing, 2010, pp. 281–304.
[9] G.M. Tsangaris, G.C. Psarras, The dielectric response of a polymeric three-component composite, J. Mater. Sci. 34 (1999) 2151–2157.
[10] J.R. Macdonald, W.B. Johnson, E. Barsoukov, J.R. Macdonald (Eds.), Impedance Spectroscopy: Theory, Experiment, and Applications, Wiley, 2005, pp. 1–26.
[11] C.J.F. Böttcher, P. Bordewijk, P. Bordewijk (Ed.)Theory of Electric Polarization, Elsevier Science Ltd, 1978, pp. 45–137.
[12] S. Nakamura, G. Sawa, M. Ieda, Electrical conduction of nylon 6 at high temperature, Jpn. J. Appl. Phys. 20 (1981) 47.
[13] N. Fuse, H. Sato, Y. Ohki, T. Tanaka, Effects of nanofiller loading on the molecular motion and carrier transport in polyamide, IEEE Trans. Dielectri. Electr. Insul. 16 (2009) 524–530.
[14] G. Kontos, A. Soulintzis, P. Karahaliou, G. Psarras, S. Georga, C. Krontiras, et al., Electrical relaxation dynamics in TiO_2-polymer matrix composites, Express Polym. Lett. 1 (2007) 781–789.
[15] A. Patsidis, G. Psarras, Dielectric behaviour and functionality of polymer matrix–ceramic $BaTiO_3$ composites, Currents 5 (2008) 10.